Use of Sparsely Distributed Synchronized Recorders for Locating Faults in Power Grids

Mert Korkalı and Ali Abur

Department of Electrical and Computer Engineering
Northeastern University,
Boston, MA 02115-5000 USA
{mkorkali, abur}@ece.neu.edu

Abstract

This study considers the use of synchronized measurements which may be few in number and possibly disbursed in a sparse manner throughout the system. An analytical derivation of a method by which location of a disturbance can be accurately determined solely based on sparsely located synchronized voltage sensors will be reviewed first. This derivation will illustrate some of the limitations and practical constraints imposed by the system topology as well as transmission-line characteristics. The paper will then build on the results of the disturbance location approach in order to devise an optimal deployment scheme for placing synchronized voltage sensors in the transmission system. This will be accomplished in such a way that any disturbance irrespective of its location can be detected and located by using as few sensors as possible. Simulated fault transients by an electromagnetic transients simulation program will be used to illustrate the performance of the developed technique.

1. Introduction

Operation of the existing power grids is rapidly being transformed due to the widespread deployment of synchronized measurement systems. These systems provide unprecedented advantages in wide-area monitoring of power grids as a result of synchronization among measurements at geographically remote parts of the system. While there are numerous studies focusing on the use of these measurements for steady-state operation and control, there have been relatively fewer investigations reported in the literature on the use of synchronized measurements for detection, characterization, and location of transient disturbances such as short-circuit faults and switching events.

This paper is intended to facilitate the utilization of synchronized measurements that are rapidly populating today's transmission grids, many of which do not have synchronized measurements at every bus, but at only "a few" selected buses. The results of this paper will enable accurate and reliable fault location by using these few strategically located synchronized measurements.

2. Review of Fault-Location Methodology [1]

A transmission grid can be represented as a graph, in which the arcs (branches) represent transmission lines and the nodes represent buses. A fault occurring on a transmission line generates a transient waveform that propagates through the network. The location of the fault can, in principle, be determined by recording the instants at which the fault waveform arrives at various points (usually buses) in the system.

We shall assume that K sensors are deployed in the network, each one measuring the time of arrival (ToA) of the fault-originated traveling wave. The data set, $\{T_k;\ 1 \leq k \leq K\}$, of these ToAs should allow us to determine:

- **(a)** which transmission line (arc) has experienced a fault;
- **(b)** at what point on this transmission line did the fault occur; and
- **(c)** the time instant at which the fault has occurred.

We discuss here only a single-fault event. In addition to the topology of the transmission grid, we also know the propagation time for each transmission line, which depends both on the length of the line and the speed of the wave propagation along the line. For a given system with L transmission lines, the propagation times, $\{D_\ell;\ 1 \leq \ell \leq L\}$, are known in advance.

The propagation delay from the point of fault occurrence to Sensor "k" depends on the network topology, the propagation times, $\{D_\ell\}$, and three unknown quantities:

- **(i)** the identity of the faulty line (say, "ℓ");
- **(ii)** the location of the fault on the line (say, αD_ℓ, from a designated end of the line, so that $0 \leq \alpha \leq 1$); and
- **(iii)** the instant, T_0, of the fault occurrence.

Thus, $T_k - T_0 = \zeta_{k\ell}(\alpha)$, which gives us an overdetermined system of equations, assuming that $K > 3$. Our challenge is to solve this system of equations for T_0, α, and ℓ.

2.1. The Functions "$\zeta_{k\ell}(\alpha)$"

Assuming that the fault occurred on Line "ℓ", the shortest propagation time from the point of fault occurrence to Sensor "k", which we denote as $\zeta_{k\ell}(\alpha)$, belongs to a path in the graph that must include one of the two endpoints (nodes) of the faulty line. We shall designate *a priori* one of these endpoints as the line ***origin*** and measure the distance to the point of fault occurrence from this end. We shall call the opposite endpoint the ***terminus*** of the line. Since we do not know in advance which endpoint of the line lies on the shortest path from the point of fault occurrence to Sensor "k", we conclude that

$$\zeta_{k\ell}(\alpha) = \min\left\{\delta_{k\ell}^{(o)} + \alpha D_\ell,\ \delta_{k\ell}^{(t)} + (1-\alpha)D_\ell\right\}, \qquad (1)$$

where $\delta_{k\ell}^{(o)}$ is the delay along the shortest path from the *origin* of Line "ℓ" to Sensor "k", and similarly, $\delta_{k\ell}^{(t)}$ is the delay along the shortest path from the *terminus* of the same line to the same sensor. The delays, $\delta_{k\ell}^{(o)}$ and $\delta_{k\ell}^{(t)}$, can be determined in advance for every "k" and every "ℓ". The pictorial representation of the described approach, along with the related terms, is highlighted in Fig. 1.

Notice that we must always have

$$\left|\delta_{k\ell}^{(o)} - \delta_{k\ell}^{(t)}\right| \leq D_\ell, \qquad (2)$$

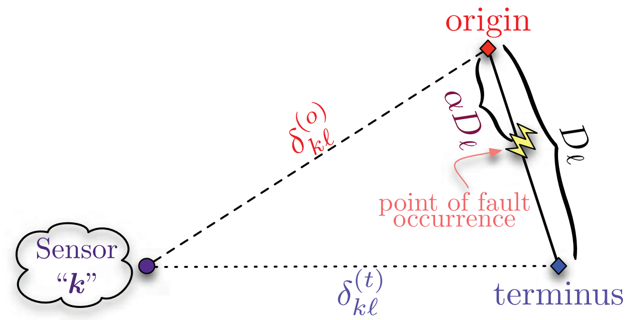

Fig. 1. Delineation of the terms "origin" and "terminus" as well as the delays, $\delta^{(o)}_{k\ell}$ and $\delta^{(t)}_{k\ell}$, with respect to Sensor "k"

so that we have

$$\delta^{(o)}_{k\ell} \le \delta^{(t)}_{k\ell} + D_\ell \quad \text{or} \quad \delta^{(t)}_{k\ell} \le \delta^{(o)}_{k\ell} + D_\ell. \tag{3}$$

A more compact expression for $\zeta_{k\ell}(\alpha)$ can be expressed in terms of $(\beta_{k\ell}, \gamma_{k\ell})$—the point where the two straight lines intersect. From

$$\delta^{(o)}_{k\ell} + \alpha D_\ell = \delta^{(t)}_{k\ell} + (1-\alpha) D_\ell, \tag{4}$$

we conclude that

$$2\alpha D_\ell = \delta^{(t)}_{k\ell} - \delta^{(o)}_{k\ell} + D_\ell \ge 0, \tag{5}$$

so that

$$\beta_{k\ell} = \frac{\delta^{(t)}_{k\ell} - \delta^{(o)}_{k\ell} + D_\ell}{2D_\ell} \tag{6a}$$

and $\beta_{k\ell} \ge 0$. Also, in view of (2), $\delta^{(t)}_{k\ell} - \delta^{(o)}_{k\ell} \le D_\ell$, so $\beta_{k\ell} \le 1$, *viz.*,

$$0 \le \beta_{k\ell} \le 1. \tag{6b}$$

Thus, the alternative expression is

$$\zeta_{k\ell}(\alpha) = \gamma_{k\ell} - |\alpha - \beta_{k\ell}| D_\ell, \tag{7}$$

where

$$\gamma_{k\ell} \triangleq \zeta_{k\ell}(\beta_{k\ell}) = \frac{\delta^{(t)}_{k\ell} + \delta^{(o)}_{k\ell} + D_\ell}{2}. \tag{8}$$

The needed network information is completely captured by the row vector

$$\mathbf{D} = \begin{bmatrix} D_1 & D_2 & \cdots & D_L \end{bmatrix} \tag{9a}$$

and the two $K \times L$ matrices

$$\mathbf{B} = \begin{bmatrix} \beta_{k\ell} \end{bmatrix} \quad \text{and} \quad \mathbf{\Gamma} = \begin{bmatrix} \gamma_{k\ell} \end{bmatrix}. \tag{9b}$$

Also, the ToA measurements on sensors generate a column vector

$$\mathbf{T} = \begin{bmatrix} T_1 & T_2 & \cdots & T_K \end{bmatrix}^{\mathrm{T}}. \tag{9c}$$

The function $\zeta_{k\ell}(\alpha)$ becomes linear when either $\beta_{k\ell} = 0$ or $\beta_{k\ell} = 1$. Both cases correspond to $\left|\delta^{(o)}_{k\ell} - \delta^{(t)}_{k\ell}\right| = D_\ell$. Indeed:

(a) When $\delta^{(o)}_{k\ell} = \delta^{(t)}_{k\ell} + D_\ell$, we get $\beta_{k\ell} = 0$ and $\gamma_{k\ell} = \delta^{(o)}_{k\ell}$.

(b) When $\delta^{(t)}_{k\ell} = \delta^{(o)}_{k\ell} + D_\ell$, we get $\beta_{k\ell} = 1$ and $\gamma_{k\ell} = \delta^{(t)}_{k\ell}$.

2.2. A Nonlinear Optimization Problem

The system of equations we need to solve is

$$\mathbf{T} - T_0 \boldsymbol{\eta} = \boldsymbol{\zeta_\ell(\alpha)}, \tag{10}$$

where

$$\boldsymbol{\eta} = \begin{bmatrix} 1 & 1 & \cdots & 1 \end{bmatrix}^{\mathrm{T}} \text{ and } \boldsymbol{\zeta_\ell(\alpha)} = \begin{bmatrix} \zeta_{1,\ell}(\alpha) & \zeta_{2,\ell}(\alpha) & \cdots & \zeta_{K,\ell}(\alpha) \end{bmatrix}^{\mathrm{T}}.$$

This system is linear in T_0, piecewise-linear in α, and highly nonlinear in the integer index "ℓ". Based on the description above, we reestablish our problem as the (constrained) optimization problem as follows:

$$\underset{\{\ell,\ \alpha,\ T_0\}}{\text{minimize}} \quad \left\| \mathbf{T} - T_0 \boldsymbol{\eta} - \boldsymbol{\zeta_\ell(\alpha)} \right\| \tag{11a}$$

$$\text{subject to} \quad 0 \le \alpha \le 1; \quad \ell \in \{1, 2, \cdots, L\}. \tag{11b}$$

2.2.1. A Two-Stage Optimization Approach

One way to solve the optimization problem (11) is to split our optimization effort into two subtasks:

(I) Fix "ℓ" and determine the optimizing T_0 and α values for the given "ℓ", say, $T_0^{(\ell)}$ and $\alpha^{(\ell)}$.

(II) Identify the value of "ℓ" that minimizes the modified cost function

$$\left\| \mathbf{T} - T_0^{(\ell)} \boldsymbol{\eta} - \boldsymbol{\zeta_\ell(\alpha^{(\ell)})} \right\|. \tag{12}$$

Selecting $\|\cdot\|$ as the Euclidean vector norm, the derivatives

$$\frac{\partial}{\partial T_0} \left\| \mathbf{T} - T_0 \boldsymbol{\eta} - \boldsymbol{\zeta_\ell(\alpha)} \right\|_2^2 \tag{13a}$$

and

$$\frac{\partial}{\partial \alpha} \left\| \mathbf{T} - T_0 \boldsymbol{\eta} - \boldsymbol{\zeta_\ell(\alpha)} \right\|_2^2 \tag{13b}$$

can be determined in closed form, allowing a closed-form expression for $T_0^{(\ell)}$ and $\alpha^{(\ell)}$. Also, in searching for ℓ, we can exclude transmission lines that are too far from the set of sensors. For instance, we can restrict our search to those arcs that are closest to the sensor with the earliest T_k.

2.2.2. A Sensor-Guided Line-Splitting Approach

One way to facilitate obtaining closed-form expressions for $T_0^{(\ell)}$ and $\alpha^{(\ell)}$ is by "linearizing" the dependence of $\zeta_{k\ell}(\alpha)$ on the variable α. This can be achieved by splitting the ℓ-th transmission line at the points defined by $\{\beta_{k\ell}\}$. We first sort the set $\{\beta_{k\ell};\ 1 \le k \le K\}$ in ascending order, say,

$$0 \le \beta_{k_1,\ell} \le \beta_{k_2,\ell} \le \cdots \le \beta_{k_K,\ell} \le 1, \tag{14}$$

and then introduce a fictitious (virtual) bus at each one of the points "$\beta_{k_i,\ell} D_\ell$" as depicted in Fig. 2.

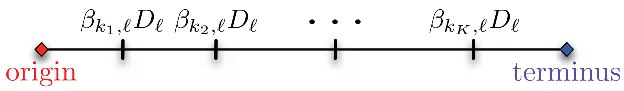

Fig. 2. The fictitious buses generated at the points "$\beta_{k_i,\ell} D_\ell$"

The number of *virtual* arcs created in that way does not exceed $K+1$. In this new graph, $\beta_{k\ell} \in \{0, 1\}$ are the only possible values for every line segment. Observe that we have now redefined "ℓ" as an index of a line segment, so that $1 \le \ell \le L_{\max}$ and $L_{\max} \le (K+1)L$. Now, $\zeta_{k\ell}(\alpha)$ is linear in α, *viz.*,

$$\begin{aligned} \zeta_{k\ell}(\alpha) &= \gamma_{k\ell} - \alpha D_\ell \\ &= \delta^{(o)}_{k\ell} - \alpha D_\ell \end{aligned} \tag{15}$$

when $\beta_{k\ell} = 0$, and

$$\begin{aligned} \zeta_{k\ell}(\alpha) &= \gamma_{k\ell} - D_\ell + \alpha D_\ell \\ &= (\delta^{(t)}_{k\ell} - D_\ell) + \alpha D_\ell \\ &= \delta^{(o)}_{k\ell} + \alpha D_\ell \end{aligned} \tag{16}$$

when $\beta_{k\ell} = 1$.

We can write this compactly as

$$\zeta_{k\ell}(\alpha) = \delta^{(o)}_{k\ell} + S_{k\ell}\alpha D_\ell, \tag{17}$$

where $S_{k\ell} = 2\beta_{k\ell} - 1 = \pm 1$.

Now, by letting $\psi = \alpha D_\ell$, our cost function becomes

$$\mathbf{J}_\ell = \left\| \boldsymbol{\delta}_\ell + \psi \mathbf{S}_\ell - \mathbf{T} + T_0 \boldsymbol{\eta} \right\|_2^2, \tag{18a}$$

where

$$\boldsymbol{\delta}_\ell = \begin{bmatrix} \delta^{(o)}_{1,\ell} & \delta^{(o)}_{2,\ell} & \cdots & \delta^{(o)}_{K,\ell} \end{bmatrix}^{\mathrm{T}} \tag{18b}$$

and

$$\mathbf{S}_\ell = \begin{bmatrix} S_{1,\ell} & S_{2,\ell} & \cdots & S_{K,\ell} \end{bmatrix}^{\mathrm{T}}. \tag{18c}$$

By setting up the equations

$$\frac{\partial \mathbf{J}_\ell}{\partial \psi} = 2\mathbf{S}_\ell^{\mathrm{T}} (\boldsymbol{\delta}_\ell + \psi \mathbf{S}_\ell - \mathbf{T} + T_0 \boldsymbol{\eta}) = 0 \tag{19}$$

and

$$\frac{\partial \mathbf{J}_\ell}{\partial T_0} = 2\boldsymbol{\eta}^{\mathrm{T}} (\boldsymbol{\delta}_\ell + \psi \mathbf{S}_\ell - \mathbf{T} + T_0 \boldsymbol{\eta}) = 0, \tag{20}$$

we obtain closed-form expressions for $\psi^{(\ell)}$ and $T_0^{(\ell)}$. The partial-derivative expressions give us

$$\begin{pmatrix} K & \mathbf{S}_\ell^{\mathrm{T}} \boldsymbol{\eta} \\ \boldsymbol{\eta}^{\mathrm{T}} \mathbf{S}_\ell & K \end{pmatrix} \begin{pmatrix} \psi^{(\ell)} \\ T_0^{(\ell)} \end{pmatrix} = \begin{pmatrix} \mathbf{S}_\ell^{\mathrm{T}} (\mathbf{T} - \boldsymbol{\delta}_\ell) \\ \boldsymbol{\eta}^{\mathrm{T}} (\mathbf{T} - \boldsymbol{\delta}_\ell) \end{pmatrix}, \tag{21}$$

which is a set of two linear equations. Rewriting the inner products as

$$\mathbf{S}_\ell^{\mathrm{T}} \boldsymbol{\eta} = \boldsymbol{\eta}^{\mathrm{T}} \mathbf{S}_\ell = \sum_{k=1}^{K} S_{k\ell}, \tag{22}$$

a "correlation coefficient" can be defined such that

$$\rho_\ell \triangleq \frac{1}{K} \sum_{k=1}^{K} S_{k\ell}, \tag{23a}$$

so that we obtain

$$K \begin{pmatrix} 1 & \rho_\ell \\ \rho_\ell & 1 \end{pmatrix} \begin{pmatrix} \psi^{(\ell)} \\ T_0^{(\ell)} \end{pmatrix} = \begin{bmatrix} \mathbf{S}_\ell & \boldsymbol{\eta} \end{bmatrix}^{\mathrm{T}} (\mathbf{T} - \boldsymbol{\delta}_\ell). \tag{23b}$$

Note that most of the quantities in the above set of equations can be calculated and stored in advance. We must evaluate only the "products" $\mathbf{S}_\ell^{\mathrm{T}} \mathbf{T}$ and $\boldsymbol{\eta}^{\mathrm{T}} \mathbf{T}$ *after* the fault has occurred and the ToAs have been measured. Indeed, these products are sums, i.e.,

$$\boldsymbol{\eta}^{\mathrm{T}} \mathbf{T} = \sum_{k=1}^{K} T_k \quad \text{and} \quad \mathbf{S}_\ell^{\mathrm{T}} \mathbf{T} = \sum_{k=1}^{K} S_{k\ell} T_k. \tag{24}$$

Referring back to the original cost function

$$\mathbf{J}_\ell = \left\| \boldsymbol{\delta}_\ell - \mathbf{T} + \begin{bmatrix} \mathbf{S}_\ell & \boldsymbol{\eta} \end{bmatrix} \begin{pmatrix} \psi \\ T_0 \end{pmatrix} \right\|, \tag{25}$$

we obtain, via (23),

$$\mathbf{J}_\ell = \left\| \mathbf{M}_\ell (\mathbf{T} - \boldsymbol{\delta}_\ell) \right\|, \tag{26a}$$

where $\mathbf{M}_\ell$ is the readily computable matrix

$$\mathbf{M}_\ell = \mathbf{I} - \frac{1}{K(1-\rho_\ell^2)} \begin{bmatrix} \mathbf{S}_\ell & \boldsymbol{\eta} \end{bmatrix} \begin{pmatrix} 1 & -\rho_\ell \\ -\rho_\ell & 1 \end{pmatrix} \begin{bmatrix} \mathbf{S}_\ell & \boldsymbol{\eta} \end{bmatrix}^{\mathrm{T}}. \tag{26b}$$

Now that the expression in (25) becomes linear in both T_0 and ψ, we can implement the two-stage optimization approach proposed in Subsection 2.2.1. The resulting modified cost function is then optimized by an integer search over a set of "ℓ" values.

In (26b), for $\rho_\ell = \pm 1$, the matrix $\mathbf{M}_\ell$ becomes noninvertible, meaning that the fault location cannot be identified on corresponding Line Segments "ℓ". Therefore, it is essential we take into account those infeasible cases before choosing the locations for synchronized sensors. In the sequel, we will introduce the formulation for the optimal placement of synchronized sensors, into which we incorporate these unsolved cases.

3. Optimal Deployment of Synchronized Sensors

Let us start by assuming that we have a synchronized voltage sensor at every bus. As a result, the number of virtual branches will be L (a number much larger than the number of lines in the original topology) after the creation of new transmission-line segments in accordance with the discussion in Subsection 2.2.2. We can then create a matrix $\boldsymbol{\mathcal{Y}}$, which contains $2L$ rows and N columns, where N is the total number buses including the virtual ones created due to the splitting of lines. Every row will contain S_{ij} as entries of $\boldsymbol{\mathcal{Y}}_{ij}$, i.e., it will either be "1" or "−1". For every (virtual) Branch i, there will be two rows, containing S_{ij} and $-S_{ij}$, respectively, for the j-th column. This provides us two inequalities, *viz.*,

$$-K < S_{i1}x_1 + S_{i2}x_2 + \cdots + S_{iN}x_N < K. \tag{27}$$

The above inequalities can be split and $\pm S_{ij}$ can be inserted in two separate rows inside the matrix $\boldsymbol{\mathcal{Y}}$, which can be built as

$$\boldsymbol{\mathcal{Y}} = \left[\begin{array}{ccccc} S_{11} & S_{12} & \cdots & \cdots & S_{1N} \\ -S_{11} & -S_{12} & \cdots & \cdots & -S_{1N} \\ \hline S_{21} & S_{22} & \cdots & \cdots & S_{2N} \\ -S_{21} & -S_{22} & \cdots & \cdots & -S_{2N} \\ \hline \cdots & \cdots & \cdots & \cdots & \cdots \\ \cdots & \cdots & \cdots & \cdots & \cdots \\ \hline S_{L1} & S_{L2} & \cdots & \cdots & S_{LN} \\ -S_{L1} & -S_{L2} & \cdots & \cdots & -S_{LN} \end{array}\right] \begin{array}{l} \left.\vphantom{\begin{array}{c} S \\ S \end{array}}\right\}\text{Branch } 1 \\ \left.\vphantom{\begin{array}{c} S \\ S \end{array}}\right\}\text{Branch } 2 \\ \vphantom{\begin{array}{c} S \\ S \end{array}} \\ \left.\vphantom{\begin{array}{c} S \\ S \end{array}}\right\}\text{Branch } L \end{array} \tag{28}$$

This will ensure that the sum of S_{ij} corresponding to those sensors placed at buses where x_j is nonzero, will not add up to K or $-K$, i.e., the corresponding virtual branch faults will be observable (detectable).

In light of these justifications, the optimization problem for sensor deployment can be explicitly formulated as

$$\begin{aligned} &\text{minimize} && \boldsymbol{\mathcal{W}}\boldsymbol{\mathcal{X}} && (29\text{a}) \\ &\text{subject to} && \boldsymbol{\mathcal{Y}}\boldsymbol{\mathcal{X}} < \boldsymbol{\mathcal{K}} && (29\text{b}) \\ & && \boldsymbol{\mathcal{X}} = [x_1 \;\; x_2 \;\; \cdots \;\; x_N]^{\mathrm{T}} && (29\text{c}) \\ & && \boldsymbol{\mathcal{K}} = [K \;\; K \;\; \cdots \;\; K]^{\mathrm{T}}_{1\times N}; \quad K \geq 0 && (29\text{d}) \\ & && x_j \in \{0, 1\} && (29\text{e}) \end{aligned}$$

where $K = \sum_{j=1}^{N} x_j$; $\boldsymbol{\mathcal{W}} = \left[w_1 \times \boldsymbol{\mathcal{U}}_{1\times n} \;\middle|\; w_2 \times \boldsymbol{\mathcal{U}}_{1\times (N-n)} \right]$; $\boldsymbol{\mathcal{U}}$ is the vector of ones; and n is the number of (actual) buses in the system. Note that we have selected $w_1 \ll w_2$ (e.g., $w_1 = 10^{-2}$ and $w_2 = 10^6$) to force the placement of maximum possible sensors on the "actual" buses rather than on the fictitious ones.

4. Practical Implementation

Our discussion in Sections 2 and 3 portrays the analytical part of our fault-location technique. Differently, we will now present the computational stages of the overall procedure along with its performance test on a transmission grid of choice.

4.1. Fundamentals and Stages of the Implementation

In order to estimate the fault point precisely, the measured voltage waveforms are initially converted to their modal components using Clarke's real transformation matrix [2]

$$\begin{pmatrix} V_o \\ V_1 \\ V_2 \end{pmatrix} = \frac{1}{\sqrt{3}} \begin{pmatrix} 1 & 1 & 1 \\ \sqrt{2} & -\frac{1}{\sqrt{2}} & -\frac{1}{\sqrt{2}} \\ 0 & \frac{\sqrt{3}}{\sqrt{2}} & -\frac{\sqrt{3}}{\sqrt{2}} \end{pmatrix} \begin{pmatrix} V_a \\ V_b \\ V_c \end{pmatrix} \tag{30}$$

since all transmission-line models are assumed to be fully transposed. Note that, in (30), V_a, V_b, and V_c denote the phase voltages; V_o is the ground-mode voltage; and V_1 and V_2 are the aerial-mode voltages. Then, the modal components are processed through the DWT and the squares of the wavelet-transform coefficients (WTC^{2}s) are retrieved and employed to detect the ToA instant of the fault-initiated traveling wave at which signal energy reaches its first local maximum. During the course of simulations, Daubechies-8 mother wavelet [3] with the level-4 approximation coefficients is chosen for the wavelet transformation. At the same time, aerial-mode voltage (e.g., V_1) WTC^{2}s in scale-1 have formed a basis for the fault-location computations.

4.2. Computation of the Shortest Propagation Delays

Recall the discussion on calculation of shortest propagation time in Subsection 2.1. For a particular bus on which a sensor is deployed, the calculation of the arrival time of the fault-initiated traveling wave to that bus is performed via (1). In the computation of the shortest propagation delay for each pair of buses, Dijkstra's well-known algorithm for shortest-path computation [4] has been employed, based on the fact that transmission grids can be regarded as undirected graphs. After the line-splitting process described in Subsection 2.2.2 is implemented, the shortest propagation delays have to be recomputed for the (fictitiously) partitioned network involving additional line segments.

4.3. Simulation Results

All simulations are carried out in ATP-EMTP program and MATLAB with a sampling frequency of 1 MHz. The fault-occurrence time is chosen to be 20 ms with respect to the simulation start time. In addition, the tower configuration of transmission lines is retrieved from [5]. Frequency-dependent transmission-line models are used in the simulations.

Before simulating the fault scenarios, all transmission lines are modeled as balanced, lossless, and fully transposed lines. The aerial-mode propagation speed in scale-1 is calculated as 1.85882×10^5 mi/s. For convenience, we assume identical configuration for each transmission line in order to eliminate the variations in traveling-wave speeds. However, the proposed method can be clearly applied to transmission grids with varying line configurations since wave-propagation time for each transmission line is computed by $D_\ell = \mathrm{d}_\ell/\nu$, where d_ℓ and ν denote the length of Line "ℓ" and the traveling-wave speed along that line, respectively. Note that the traveling-wave speeds can be extracted based on the knowledge of the electrical characteristics of all transmission lines in the power grid. Transmission-line lengths, along with wave-propagation times, are provided in Table 1.

Table 1. Line lengths and propagation times for the studied system

Line	Length (mi)	Time (μs)	Line	Length (mi)	Time (μs)
$1-2$	262	1,409.50	$12-13$	25	134.49
$1-3$	85	457.28	$12-14$	211	1,135.13
$2-4$	138	742.41	$12-15$	127	683.23
$2-5$	134	720.89	$12-16$	261	1,404.12
$2-6$	195	1,049.05	$14-15$	262	1,409.50
$3-4$	316	1,700.00	$15-18$	66	355.06
$4-6$	321	1,726.90	$15-23$	32	172.15
$4-12$	82	441.14	$16-17$	166	893.04
$5-7$	37	199.05	$18-19$	232	1,248.10
$6-7$	49	263.61	$19-20$	67	360.44
$6-8$	10	53.80	$21-22$	154	828.48
$6-9$	276	1,484.81	$22-24$	149	801.58
$6-10$	219	1,178.17	$23-24$	312	1,678.48
$6-28$	61	328.17	$24-25$	152	817.72
$8-28$	19	102.22	$25-26$	174	936.08
$9-10$	246	1,323.42	$25-27$	106	570.25
$9-11$	122	656.33	$27-28$	173	930.70
$10-17$	251	1,350.32	$27-29$	275	1,479.43
$10-20$	103	554.12	$27-30$	267	1,436.40
$10-21$	219	1,178.17	$29-30$	218	1,172.79
$10-22$	186	1,000.63			

Now, consider the modified IEEE 30-bus system whose single-line diagram is depicted in Fig. 3. We simulate a short-circuit fault at the point 73 miles away from Bus 2 on the 195-mile-long transmission line connecting Buses 2 and 6. Aerial-mode WTC^{2}s for each modal voltage are obtained following the decoupling of the three-phase synchronized voltage measurements into the modal voltages. Two of these voltage measurements and the pertinent aerial-mode voltage WTC^{2}s are illustrated in Fig. 4.

The strategically selected locations for the synchronized recorders in the studied network are listed in Table 2. The table also illustrates the instants when the first local peaks of WTC^{2}s are detected via the synchronized recorders on the respective buses. Hence, the captured times in milliseconds are stored in the (11×1)-column vector $\mathbf{T}$ right after the occurrence of the fault. After the optimal placement of the synchronized recorders, the regenerated network consists of 102 buses and 113 transmission-

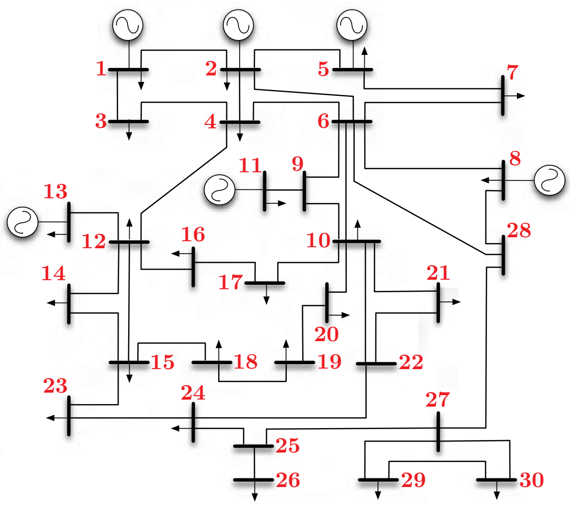

Fig. 3. Single-line diagram of the modified IEEE 30-bus test system

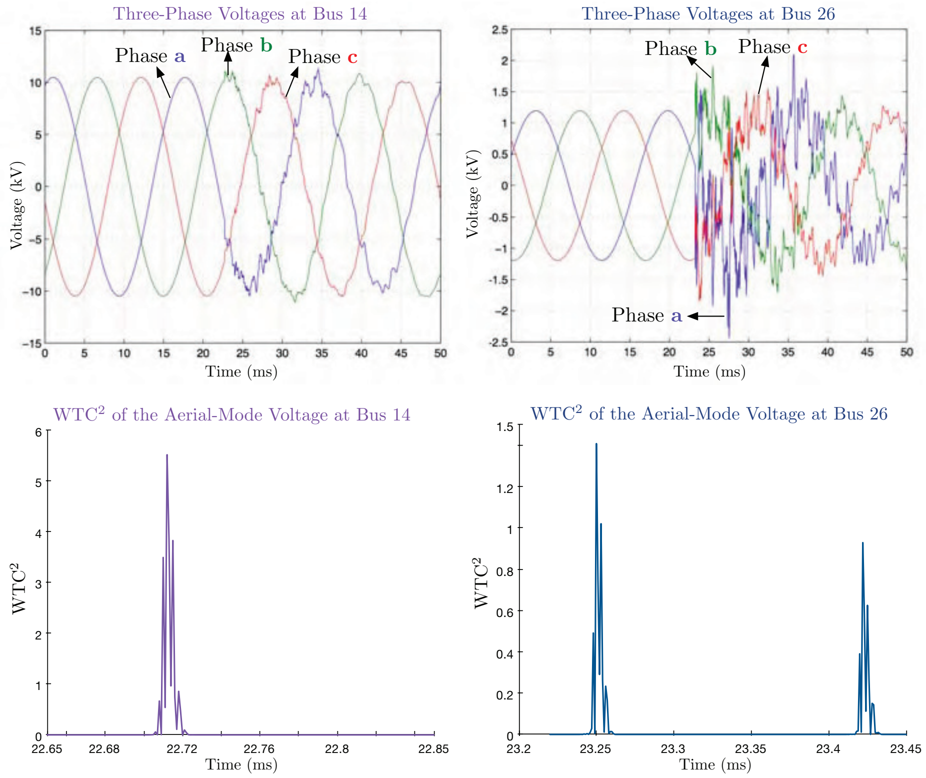

Fig. 4. Phase voltages and WTC^{2}s of the aerial-mode voltages at Buses 14 and 26 after the occurrence of a short-circuit fault on Line 2-6

Table 2. Synchronized meter locations *versus* wave-arrival times for the short-circuit fault occurring on Line 2-6

Buses	**3**	**5**	**6**	**11**	**13**	**14**	**17**	**21**	**26**	**29**	**30**
ToAs (ms)	22.254	21.113	20.654	22.794	21.708	22.708	23.184	23.008	23.248	23.216	23.176

line segments with the inclusion of virtual nodes and arcs.

For the fault-scenario example above, the minimizing value of the cost function, i.e., $J_{22} = 0.0056 \approx 0$, is attained on Line 22 in the resulting split network, after labeling the line segments. As a result, the corresponding values of $\psi^{(\ell)}$ and $T_0^{(\ell)}$ are found to be

$$\begin{pmatrix} \psi^{(22)} \\ T_0^{(22)} \end{pmatrix} = \begin{pmatrix} 0.3443 \\ 19.9971 \end{pmatrix} \quad \text{ms.}$$

In Fig. 5, the location of the fault on Line 2-6 is displayed in terms of the propagation delay, $\psi^{(\ell)}$, associated with the fault. As illustrated in the figure, the location of the fault is detected on the virtual line segment (i.e., Line 22) connecting Terminals 43 and 44. The numbers shown right below these line segments represent the calculated propagation times (in milliseconds). The distance to fault from Bus 2 is thus computed to be

$$\begin{aligned} \widehat{d} &= \left((0.484 + 3.443) \times 10^{-4} \text{ s}\right) \times (1.85882 \times 10^5 \text{ mi/s}) \\ &= 72.9959 \approx 73 \text{ mi.} \end{aligned}$$

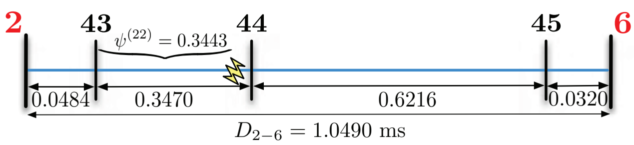

Fig. 5. The value of $\psi^{(\ell)}$ for the short-circuit fault occurring on Line 2-6

5. Concluding Remarks

The fault-location method proposed in this paper utilizes a few and dispersedly placed synchronized measuring devices with the aim of locating any fault in a transmission network regardless of where it is originated. In particular, we introduce one possible method employing synchronized voltage measurements for optimal sensor deployment, thereby ascertaining system observability in the sense of disturbance location. Being contingent upon GPS-synchronized sampling of transient voltage signals, the developed procedure entails the extraction of time-of-arrival values determined by DWT-based processing of faulted voltage waveforms.

Acknowledgment

This work was supported in part by Grant #2574520-47177-A from the Global Climate and Energy Project (GCEP) at Stanford University.

6. References

[1] M. Korkalı, H. Lev-Ari, and A. Abur, "Traveling-wave-based fault-location technique for transmission grids via wide-area synchronized voltage measurements," *IEEE Trans. Power Syst.*, submitted for publication.

[2] E. Clarke, *Circuit Analysis of AC Power Systems, Symmetrical and Related Components*. New York: Wiley, 1943.

[3] I. Daubechies, *Ten Lectures on Wavelets*. Philadelphia: PA: SIAM, 1992.

[4] E. W. Dijkstra, "A note on two problems in connexion with graphs," *Numerische Mathematik*, vol. 1, pp. 269–271, 1959.

[5] C. Y. Evrenosoğlu and A. Abur, "Travelling wave based fault location for teed circuits," *IEEE Trans. Power Del.*, vol. 20, no. 2, pp. 1115–1121, Apr. 2005.